On the Origin of Stationary Electroosmotic Flow Driven by AC Fields Around Insulators

Víctor Calero,[1,*] Raúl Fernández-Mateo,[1,*] Hywel Morgan,[1] Pablo García-Sánchez,[2] and Antonio Ramos[2,†]

[1] *School of Electronics and Computer Science, University of Southampton, United Kingdom.*
[2] *Depto. Electrónica y Electromagnetismo. Facultad de Física. Universidad de Sevilla. Avda. Reina Mercedes s/n, 41012. Sevilla (Spain).*

(Dated: March 2, 2021)

Electric fields are commonly used for manipulating particles and liquids in microfluidic systems. In this work, we report stationary electroosmotic flow vortices around dielectric micro-pillars induced by AC electric fields in electrolytes. The flow characteristics are theoretically predicted based on the well-known phenomena of surface conductance and concentration polarization around a charged object. The stationary flows arise from two distinct contributions working together: an oscillating non-uniform zeta-potential induced around the pillar and a rectified electric field induced by the ion concentration gradients. We present experimental data in support of the theoretical predictions. The magnitude and frequency dependence of the electroosmotic velocity are in agreement with the theoretical estimates and are significantly different from predictions based on the standard theory for induced-charge electroosmosis, which has previously been postulated as the origin of the stationary flow around dielectric objects. In addition to furthering our understanding of the influence of AC fields on fluid flows, we anticipate that this work will also expand the use of AC fields for flow control in microfluidic systems.

Keywords: AC Electrokinetics, Microfluidics, Electroosmosis, Surface Conductance, Concentration Polarization.

I. INTRODUCTION

Solid surfaces in contact with aqueous electrolytes usually carry a net surface charge arising from the different affinities of cations and anions [1]. This surface charge is screened by a diffuse ionic layer on the electrolyte side of the interface, and liquid streaming can occur when an external electric field acts on these charges. This fluid flow is known as electroosmosis (EO) [2] and is a common way of driving liquids within capillaries and microfluidic structures [3]. The thickness of the diffuse layer (Debye length) for typical aqueous electrolytes is around tens of nanometers or smaller [1]. Thus, at length scales of micrometers or larger, the fluid motion that occurs within the diffuse layer can be modelled via an effective slip velocity tangential to the solid wall, $\mathbf{u}_{\text{slip}}$. The Helmholtz-Smoluchowski formula relates the slip velocity with the applied electric field ($\mathbf{E}$) and the zeta potential (ζ) of the interface [1]:

$$\mathbf{u}_{\text{slip}} = -\frac{\varepsilon\zeta}{\eta}\mathbf{E}, \tag{1}$$

where ε and η are, respectively, the electrolyte permitivitty and viscosity. The zeta potential is commonly defined as the electrical potential at the slip plane with the bulk solution [4].

In the case of AC electric fields, eq. (1) predicts an oscillating slip velocity with a zero time-average value. However, recent experimental reports have shown a non-zero time-average slip velocity of electrolytes around dielectric pillars in an AC field [5]. Similar stationary (or rectified) flows have been observed around dielectric corners [6–8] and have been attributed to induced-charge electroosmosis (ICEO) [9], i.e. electroosmosis generated by the action of an electric field on the charges in the diffuse layer induced by the same field [10], see figure 1(a). In this work we show that ICEO is not the origin of these flows and demonstrate that a rectified fluid

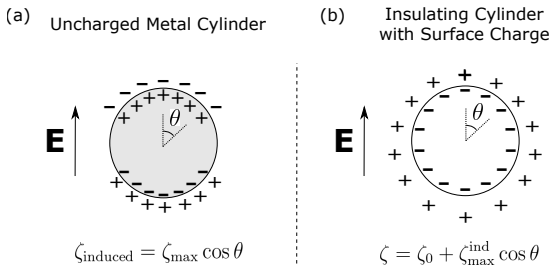

FIG. 1. (a) An applied electric field induces charges on a metal (conducting) cylinder that are screened by ions in the liquid phase – a diffuse layer is induced around the metal object. ICEO occurs due to the action of the applied field on these diffuse-layer charges. (b) A dielectric cylinder has an intrinsic surface charge. Upon application of an electric field, surface conductance creates both a non-homogeneous electrolyte concentration and zeta potential around the cylinder. In (b), the distance of the positive ions (counterions) to the particle surface changes with position - this indicates that the Debye length varies due to concentration polarization. For both (a) and (b), and using equation (1), the induced zeta potentials generate stationary quadrupolar flows around the cylinder.

* Both authors contributed equally to this work.
† Corresponding author: ramos@us.es

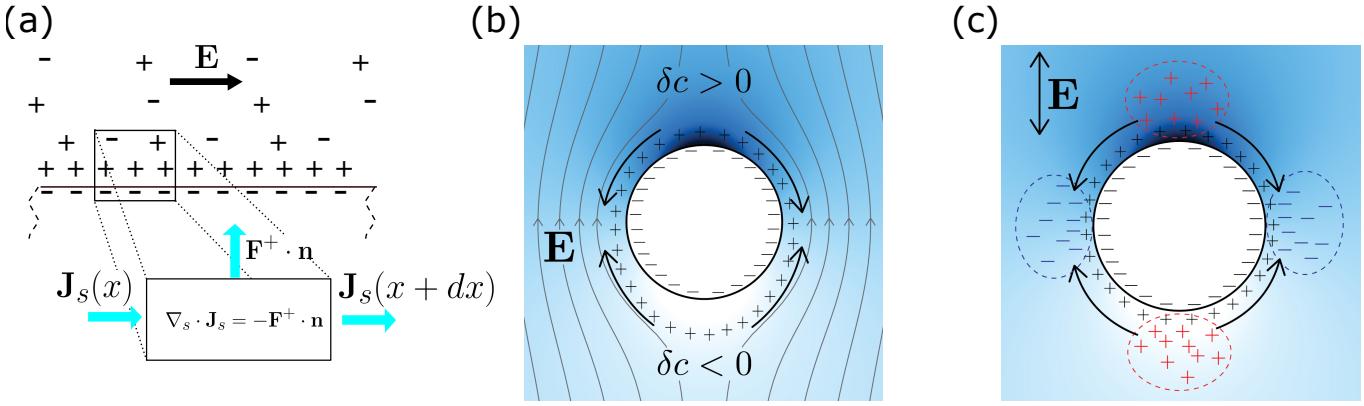

FIG. 2. (a) Negative charges on the dielectric surface attract (positive) counterions. The mean ion concentration increases near the surface leading to a surface current density $\mathbf{J}_s$. Charge conservation implies that variations in surface current must be balanced by a counterion flux ($\mathbf{F}^+$). (b) Color map showing the perturbation in electrolyte concentration (δc) around a charged cylinder. Darker blue indicates a higher value of c. As a consequence of the concentration polarization, the screening thickness (Debye length) depends on position around the cylinder. The black arrows indicate the direction of the stationary electroosmotic flow. (c) A consequence of concentration polarization is induced free charge that is in addition to the concentration gradients. The rectified electric field due to these charges acts on the diffuse-layer charges and generates an electroosmotic flow.

flow arises from the polarization of modified electrolyte concentration (i.e. concentration polarization) that results from the surface conductance around a dielectric pillar [2].

Figure 1(b) shows a diagram of how concentration polarization (CP) leads to a non-homogeneous zeta potential. We have assumed that the pillar carries a negative intrinsic surface charge density (q_s) which is linked to ζ via the Gouy-Chapman equation $q_s = 2\sqrt{2c\varepsilon e\phi_{\rm ther}}\sinh(\zeta/2\phi_{\rm ther})$, with c the electrolyte concentration and $\phi_{\rm ther} = k_{\rm B}T/e$ the thermal voltage ($k_{\rm B}$ is Boltzmann's constant, T absolute temperature and e the proton charge; $\phi_{\rm ther} \approx 25\,{\rm mV}$ at $20^{\rm o}$C) [1]. A consequence of the surface charge is a local increase in counterion concentration within the diffuse layer and an accompanying enhancement in electrical conductivity that manifests itself as a surface conductance that is in addition to the bulk electrolyte conductivity [2], see Figure 2(a). When an external electric field acts on the interface, the additional current near the wall leads to depletion of electrolyte on one side of the pillar, and a corresponding enhancement on the opposite side. Figure 2(b) depicts the variation in electrolyte concentration that appears near a charged cylinder subjected to an external electric field. Thus, the electrolyte concentration near the wall is not homogeneous and since q_s is fixed, the Gouy-Chapman relation implies that ζ also varies over the solid wall. The effects of CP on colloids have been extensively studied [11–13]; it is responsible for the well-known low-frequency dispersion of a colloidal suspension - the so called α-relaxation.

In the following sections we focus on developing a theoretical model for the effect of CP on the electroosmotic slip velocity induced by an AC electric field around an insulating pillar. We show that two distinct mechanisms acting together give rise to stationary flows: an oscillating non-uniform zeta-potential and a rectified electric field induced by the concentration gradients. We also present experimental data of these stationary flows. Both the magnitude and frequency dependence of the electroosmotic velocity are in agreement with the theoretical estimates and differ significantly from predictions based on the theory for induced-charge electroosmosis.

II. THEORY

Our analysis for an insulating cylinder follows the work of Schnitzer and Yariv [14, 15] for the electrophoresis of charged particles immersed in a symmetrical electrolyte. We extend their analysis to the case of AC signals (see appendix A for details). We perform a linear expansion of the governing equations for small Dukhin number (Du); the ratio of surface to bulk conductance [2]. The linearization of the electrokinetic equations for ac voltages gives rise to a steady velocity field that scales linearly with Du but is quadratic with the amplitude of the electric field. In the approximation, the electrical potential is written as $\phi = \phi_0 + \delta\phi$, where ϕ_0 is the potential around a dielectric cylinder for Du = 0, and $\delta\phi$ is the perturbation as a consequence of surface conductance. ϕ_0 satisfies Laplace equation with zero normal derivative as the boundary condition on the cylinder surface. For an applied AC field of magnitude E_0 and angular frequency ω, ϕ_0 can be written as $\phi_0(t) = \mathcal{R}e[\tilde{\phi}_0 \exp(i\omega t)]$, where $\mathcal{R}e[\cdots]$ means the real part of the function between the brackets and $\tilde{\phi}_0$ is the potential phasor, which

in cylindrical coordinates is written as:

$$\tilde{\phi}_0 = -E_0 \left(r + \frac{a^2}{r} \right) \cos\theta. \tag{2}$$

Likewise, the salt concentration can be written as $c = c_0 + \delta c$, where c_0 is the bulk concentration and δc is the perturbation due to the applied field. For a relatively small surface conductance, and neglecting advection, δc is given by the solution of the diffusion equation:

$$D\nabla^2 \delta c = \partial_t \delta c, \tag{3}$$

where D is the diffusion coefficient of the ions in the electrolyte.

For thin diffuse layers, the ion flux balance shown in Figure 2(a) can be written as an effective boundary condition that incorporates the surface conductance as a parameter. Assuming that negative ions (co-ions) are expelled from the diffuse layer, the divergence of the surface current must be balanced by the normal flux of positive ions. The boundary condition for δc on the insulating surface is written as [15]:

$$-\mathbf{n} \cdot \nabla \delta c / c_0 = \mathrm{Du}\, a \nabla_s^2 (\phi_0/\phi_{\mathrm{ther}}), \tag{4}$$

where $\mathbf{n}$ is a unit vector normal to the wall, a is the cylinder radius and ϕ_0 is the electrical potential. ∇_s^2 is the Laplacian operator tangential to the wall surface. As mentioned above, Du is the ratio of surface to bulk conductance ($\mathrm{Du} = K_s/a\sigma$, with K_s the surface conductance and σ the electrolyte conductivity).

δc is also an oscillating function with angular frequency ω and with a frequency-dependent phasor given by:

$$\delta\tilde{c}/c_0 = -2\mathrm{Du} \frac{E_0 a}{\phi_{\mathrm{ther}}} \frac{K_1(kr)}{kaK_1'(ka)} \cos\theta, \tag{5}$$

where $k = \sqrt{i\omega/D}$, $K_n(x)$ is the modified Bessel function of the second kind of order n and $K_n'(x) = dK_n/dx$. The relaxation angular frequency for δc is the reciprocal of the typical time in the diffusion equation, $\tau = a^2/D$. Figure 2(b) shows the solution for δc around a cylinder for $\omega = 0$, i.e. a DC field.

According to the Gouy-Chapman relation, a change in local concentration δc implies a perturbation in zeta potential given by $\delta\zeta/\phi_{\mathrm{ther}} = -\delta c|_{r=a} \tanh(\zeta_0/2\phi_{\mathrm{ther}})/c_0$ and thus, ζ can be written as shown in Figure 1(b). For the case of an AC excitation, the inhomogeneous part of ζ is an oscillating function with angular frequency ω. Using the Helmholtz-Smoluchowski equation, it can be readily shown that a non-zero time-averaged electroosmotic velocity appears, given by:

$$\langle \mathbf{u}_{\mathrm{slip}} \rangle_{\mathrm{A}} = (\varepsilon/2\eta) \mathcal{R}e[\delta\tilde{\zeta} \nabla_s \tilde{\phi}_0^*], \tag{6}$$

where * indicates complex conjugate. Grosse and Shilov [16, 17] proposed a similar mechanism as the explanation for the co-field electrorotation observed in polystyrene microspheres at low frequencies (below 100 Hz).

Another effect of the concentration polarization is the induction of a net electrical charge arising from the concentration gradients [18, 19]. In fact, current conservation for a symmetrical electrolyte leads to the following equation for the perturbation of the electrical potential, $\nabla^2 \delta\phi = -\nabla\phi_0 \cdot \nabla\delta c/c_0$ (see Appendix A). Since δc and ϕ_0 are oscillating functions with angular frequency ω, $\delta\phi$ has a non-zero time-averaged component satisfying:

$$\nabla^2 \langle \delta\phi \rangle = -(1/2) \mathcal{R}e[\nabla\tilde{\phi}_0 \cdot \nabla\delta\tilde{c}^*/c_0]. \tag{7}$$

Figure 2(c) shows a schematic representation of the induced charges associated with the rectified potential ($\delta\rho = -\varepsilon\nabla^2\langle\delta\phi\rangle$) for a cylinder with negative surface charge. The rectified electric field corresponding to these induced charges acts on the intrinsic charges of the diffuse layer generating an electroosmotic slip velocity with non-zero time average given by:

$$\langle \mathbf{u}_{\mathrm{slip}} \rangle_{\mathrm{B}} = (\varepsilon/\eta)\zeta_0 \nabla_s \langle\delta\phi\rangle. \tag{8}$$

To the best of our knowledge, this contribution to the slip velocity has not been previously considered.

Evaluation of eq. 8 requires a solution for $\langle\delta\phi\rangle$. To this end, we write equation (7) as:

$$\nabla^2 \langle\delta\phi\rangle/\phi_{\mathrm{ther}} = \mathrm{Du}(E_0 a/\phi_{\mathrm{ther}})^2 \mathcal{R}e[f(r) + g(r)\cos(2\theta)], \tag{9}$$

where

$$f(r) = \frac{1}{2K_1'(ka)} \left(K_0(kr) - \frac{K_2(kr)}{(r/a)^2} \right), \tag{10}$$

$$g(r) = \frac{1}{2K_1'(ka)} \left(K_2(kr) - \frac{K_0(kr)}{(r/a)^2} \right). \tag{11}$$

From this the solution is $\langle\delta\phi\rangle/\phi_{\mathrm{ther}} = \mathrm{Du}(E_0 a/\phi_{\mathrm{ther}})^2 \mathcal{R}e[F(r) + G(r)\cos(2\theta)]$. $G(r)$ is the only function that contributes to the slip velocity (the derivation of $G(r)$ is outlined in the appendices). Thus, the combination of the contributions given by eqs. (6) and (8) provides the rectified slip velocity for the cylinder. This is of the form $\langle u_{\mathrm{slip}} \rangle = U \sin(2\theta)$, with U the frequency dependent, maximum slip velocity:

$$\frac{U}{(\varepsilon a E_0^2/2\eta)\mathrm{Du}} = (1/2)|\zeta_0| f_1 + 2\tanh(|\zeta_0|/2) f_2, \tag{12}$$

where we define the functions f_1 and f_2 as

$$f_1(\omega a^2/D) = 4\mathcal{R}e[G(a)], \tag{13}$$

$$f_2(\omega a^2/D) = -\mathcal{R}e[K_1(ka)/(kaK_1'(ka))]. \tag{14}$$

The functions $f_1(x)$ and $f_2(x)$ are plotted in figure 3. For zero frequency ($k = 0$), $f_1 = f_2 = 1$ and

$$\frac{U}{(\varepsilon a E_0^2/2\eta)\mathrm{Du}} = |\zeta_0|/2 + \tanh(|\zeta_0|/2), \tag{15}$$

while for high frequencies $f_1 \ll f_2$ and

$$\frac{U}{(\varepsilon a E_0^2/2\eta)\mathrm{Du}} \sim \frac{1}{\sqrt{2\omega a^2/D}} \tanh(|\zeta_0|/2). \qquad (16)$$

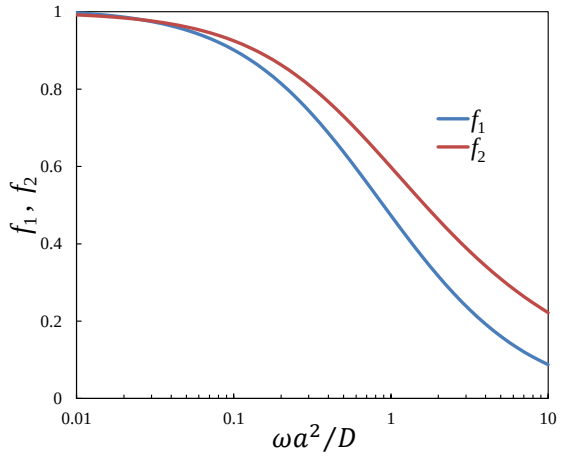

FIG. 3. Plot of the functions f_1 and f_2 versus $\omega a^2/D$. The frequency dependence of the slip velocity is contained within these functions (eq. (12)).

The rectified slip velocity gives rise to a quadrupolar flow of the liquid around the cylinder with a velocity field given by:

$$\langle \mathbf{u} \rangle = U \left(\frac{1-r^2}{r^3} \cos(2\theta)\hat{r} + \frac{1}{r^3} \sin(2\theta)\hat{\theta} \right). \qquad (17)$$

This expression gives rise to a velocity amplitude that approximately decays as $\sqrt{D/\omega a^2}$ at frequencies larger than D/a^2. ICEO flows around a cylinder are also quadrupolar (they satisfy eq. (17)) and scale with E_0^2 [20]. However, assuming that the permittivity of the cylinder is much smaller than that of water (true for all experimental cases), the ICEO theory predicts a velocity with a frequency dependence consisting of a plateau followed by a decay around frequencies of the order of the reciprocal of the charge relaxation time of the electrolyte ($\sigma/(2\pi\varepsilon) \approx 0.3 - 3\,\mathrm{MHz}$ for our experimental conditions. This frequency is several orders of magnitude greater than the typical frequencies for the flows observed in our experiments [9, 21]). It is also enlightening to compare the slip velocities predicted by both theories. According to ICEO theory for dielectric objects [20, 22], the maximum induced zeta potential for a DC field with amplitude E_0 is $\delta\zeta_{\mathrm{ICEO}} = 2(\varepsilon_d/\varepsilon)E_0\lambda_D$, where ε_d is the permittivity of the dielectric object and λ_D the thickness of the diffuse layer, i.e. the Debye length. Thus, from eq. (1), the maximum time-averaged slip velocity for an AC field of amplitude E_0 is $v_{\mathrm{slip}}^{\mathrm{ICEO}} = (\varepsilon_d/\eta)\lambda_D E_0^2$. On the other hand, the maximum slip velocity for the stationary flows is

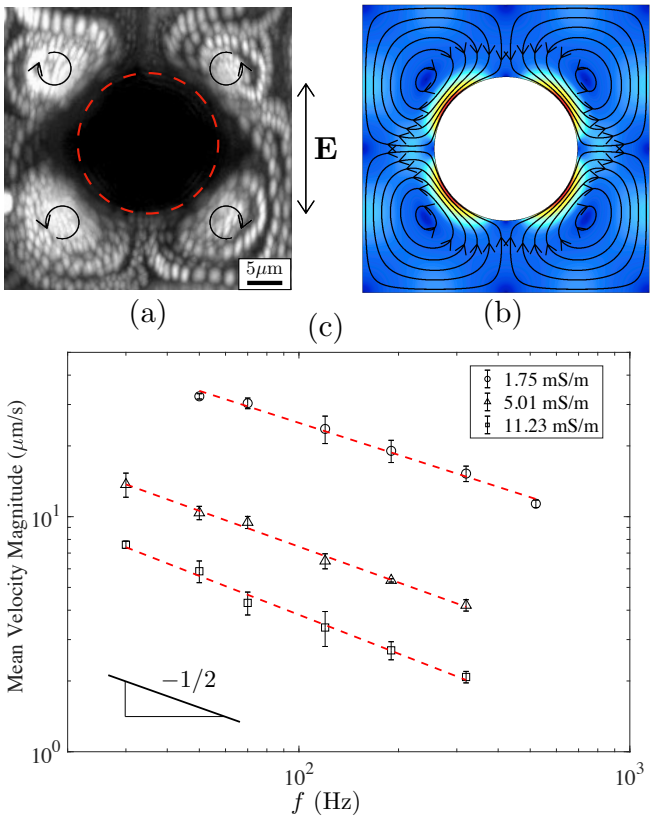

FIG. 4. (a) Experimental streamlines around an insulating pillar of 20 μm diameter. The electrolyte conductivity was 1.75 mS/m and the voltage amplitude and frequency were 1600 V_{pp} and 190 Hz, respectively (see video in supplementary material [23]). (b) Numerically calculated streamlines for the rectified electroosmotic flow around a dielectric cylinder. The color map represents the magnitude of the fluid velocity field. (c) Experimental data for the average fluid velocity magnitude as a function of signal frequency for three electrolyte conductivities (KCl in water). The amplitude of the applied voltage is 1600 V_{pp}. The velocity approximately decays as $1/\sqrt{f}$.

$v_{\mathrm{slip}}^{\mathrm{CPEO}} = (\varepsilon a E_0^2/2\eta)\mathrm{Du}(|\zeta_0|/\phi_{\mathrm{ther}} + 2\tanh(|\zeta_0|/2\phi_{\mathrm{ther}}))$, where we introduce the acronym CPEO for concentration polarization electroosmosis. Using values of the parameters obtained from our experiments, and typical values for the permittivity of PDMS ($\varepsilon_d = 2.8\varepsilon_0$), $\lambda_D \leq 30\,\mathrm{nm}$ and $\mathrm{Du} \in [0.01, 0.1]$, the ratio between the two slip velocities is $v_{\mathrm{slip}}^{\mathrm{ICEO}}/v_{\mathrm{slip}}^{\mathrm{CPEO}} \in [0.004, 0.04]$, which demonstrates that CPEO stationary flows completely dominate over ICEO for charged dielectric obstacles.

III. EXPERIMENTAL RESULTS AND COMPARISON WITH THEORY

The CPEO flows were experimentally validated using simple microfluidic devices made using standard soft

lithography. Channels (1 cm long, 50 μm tall, 200 μm wide) containing a periodic square array of cylindrical micropillars (20 μm diameter) were made from PDMS. The separation between the centers of neighboring pillars was 40 μm. The channel was filled with KCl electrolyte with conductivities $\sigma = \{1.75, 5.01, 11.23\}$ mS/m. For flow visualization, fluorescent nanoparticles (500 nm diameter) were dispersed in the electrolyte and imaged with a fluorescence microscope. Before experiments, the PDMS channels were primed for at least 30 minutes with a solution of 0.1% Pluronics F-127 – a non-ionic surfactanct that adsorbs onto the PDMS walls to minimise sticking of the tracer particles. Metal needles were inserted at the inlet and outlet of the channel and AC voltages applied, with amplitude up to 2000 V_{pp} and frequencies up to 1 kHz. Videos of the fluorescent particles were analyzed with Particle Image Velocimetry (PIV) (described in section S3 of supplementary material [23]).

Figure 4(a) shows results of the superposition of experimental images showing the trajectories of the fluorescent particles in an electrolyte. Four symmetrical flow rolls are seen, as predicted from the theory for the rectified electroosmotic flow field around a cylinder. Figure 4(c) shows the mean value of the velocity magnitude as a function of the applied AC frequency for three electrolyte conductivities. Following convention, the frequency in experiments f is related to the angular frequency by $\omega = 2\pi f$. The data were obtained by averaging the fluid velocity magnitude within a unit cell of the periodic array of cylinders. Error bars correspond to the dispersion in the measurements within six different unit cells. Importantly, a strong decrease of the stationary velocity is observed for frequencies around and above tens of Hertz, in accordance with $a^2/D \approx 0.1$ s, i.e. the timescale introduced by the diffusion equation, eq. (3). Additionally, the velocity for a given conductivity approximately decays as $1/\sqrt{f}$, also in agreement with theoretical predictions. We have also performed experiments using a single post (rather than an array). The observed flow is completely analogous to the flow observed with the array of posts. An example of streamlines is shown in section S1 of supplementary material [23].

The stationary electroosmotic velocity for a periodic array of dielectric cylinders as used experimentally was calculated using the commercial finite element solver COMSOL Multiphysics. The governing equations for ϕ_0 (Laplace equation), δc (eq.(3)) and $\langle\delta\phi\rangle$ (eq. (7)) were solved in a 2D domain corresponding to a unit cell centered on a cylinder, see Figure 4(b). Boundary conditions on the cylinder surface were $\mathbf{n}\cdot\nabla\phi_0 = 0$, eq.(4) and $\mathbf{n}\cdot\nabla\langle\delta\phi_0\rangle = 0$. Periodicity was imposed on the boundaries of the unit cell. The velocity field within the unit cell satisfies Stokes equations with slip velocity on the cylinder wall given by the sum of eqs. (6) and (8). We also imposed periodicity for the velocity and pressure fields on the boundaries of the unit cell.

Figure 4(b) shows the streamlines obtained for the rectified electroosmotic flow around a post in the periodic array. As expected, the time-averaged flow pattern shows four recirculating vortices as found experimentally. Fig. 5 shows a comparison between the experimental data from figure 4(c) and numerical results with the following parameters: $\zeta_0 = -110$ mV (for the lowest conductivity) [24] and $E_0 = 96.25$ kV/m. For the other conductivities, ζ_0 was calculated from the Gouy-Chapman relation for fixed surface charge; these values are in agreement with the measurements in [25]. The experimental data in fig. 5 are scaled with u_0Du, where $u_0 = \varepsilon a E_0^2/2\eta$ and Du is calculated by assuming a fixed surface conductance of 1 nS – independent of electrolyte conductivity. This is a typical value obtained from experimental data for the electrokinetic properties of submicrometre latex particles [26] and it is larger that the estimation obtained for K_s when using the theory of the diffuse layer. The difference is attributed to the contribution to surface conductance arising from a layer of mobile ions adsorbed on the wall [12] – the so-called Stern layer. Experimental trends are correctly described by the theoretical model: the rectified fluid

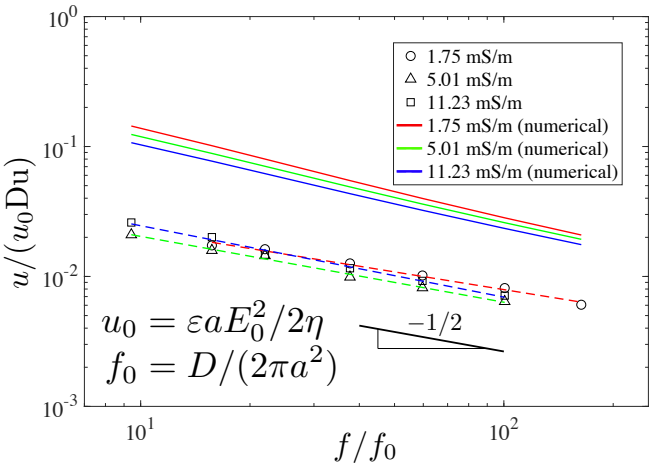

FIG. 5. Comparison between experimental data in figure 4(c) and numerical calculations for a periodic array of dielectric cylinders. The solid lines correspond to the average velocity magnitude determined from simulations with $E_0 = 96.25$ kV/m and $\zeta_0 = -110$ mV for the lowest conductivities. For the other conductivities, ζ_0 was calculated from the Gouy-Chapman relation for fixed surface charge. Frequencies are nondimensionalized with $f_0 = D/(2\pi a^2)$. Velocities are scaled with the product of a typical velocity ($u_0 = \varepsilon a E_0^2/2\eta$) and the Dukhin number. Note that the numerical curves do not exactly have the same frequency dependence and, therefore, they do not collapse onto a master curve. The reason is that the relative contribution of the two mechanisms to rectified electroosmosis varies with ζ_0, which in turn decreases with electrolyte conductivity.

velocity decreases with electrolyte conductivity and, significantly, its frequency dependence is close to $1/\sqrt{f}$. The magnitude of the velocity is clearly overestimated by the numerical simulations by a factor of around 4.5. It is important to note that the channels were primed with the surfactant Pluronics before each experiment which is known to significantly reduce electroosmotic velocities [27].

IV. CONCLUSIONS

We have presented a mathematical model that predicts stationary fluid flow of electrolytes induced by AC electric fields around charged dielectric objects. We show experimental data for electrolyte flow around micropillars in a microfluidic channel and demonstrate that the experimental trends are in agreement with numerical calculations for typical values of surface conductance and ζ-potential for PDMS.

The magnitude of the fluid velocity is overestimated by the numerical calculations which can be attributed to the fact that adsorption of Pluronics to PDMS significantly reduces electroosmosis. The theoretical model correctly describes the amplitude and frequency dependence of the rectified flow, in contrast with previous work that attributes the flow around dielectric structures to classical ICEO in an AC field [9, 28]. Beyond the fundamental interest in these stationary flows, we anticipate that this model will expand the understanding of the behavior of systems that employ AC electric fields for micro- and nanoparticle manipulation [29, 30] and lead to ways of locally controlling fluid flow using dielectric structures.

ACKNOWLEDGMENTS

PGS and AR acknowledge financial support by ERDF and Spanish Research Agency MCI under contract PGC2018-099217-B-I00.

Appendix A: Theory for Surface Conductance and Electroosmosis

We consider a negatively charged dielectric object immersed in a binary electrolyte subjected to an AC electric field and follow the theory developed by Schnitzer and Yariv [14], but extending it to the AC case. This theory is a thin-double-layer analysis of the electrokinetic equations for charged dielectric solids that considers surface conduction effects. We assume that the frequency ω of the applied electric field is low enough to consider the EDL is in quasi-equilibrium ($\omega\varepsilon/\sigma \ll 1$, with ε and σ, the liquid permittivity and conductivity, respectively). In the following we use a dimensionless formulation [14]: length is nondimensionalised with a typical distance a (radius of the pillar in our experiments), potential with the thermal voltage $\phi_{\rm ther} = k_{\rm B}T/e$ ($k_{\rm B}$ is Boltzmann's constant, T absolute temperature and e elementary charge), time with $\eta/\varepsilon E_{\rm ther}^2$ where $E_{\rm ther} = \phi_{\rm ther}/a$, pressure with $\varepsilon E_{\rm ther}^2$, and concentrations with typical salt concentration c_0. Thus, diffusion constants are nondimensionalised with $\varepsilon a^2 E_{\rm ther}^2/\eta$, velocities with $\varepsilon E_{\rm ther}^2 a/\eta$, and the typical Reynolds number is $\mathrm{Re} = \rho_m \varepsilon E_{\rm ther}^2 a^2/\eta^2$, with ρ_m the liquid mass density. The surface charge on the dielectric is nondimensionalised with $\varepsilon\phi_{\rm ther}/\lambda_D$, where λ_D is the Debye length.

The nondimensional equations for the conservation of positive and negative ions in the bulk electrolyte (outside the electrical double layer) are, respectively,

$$\nabla\cdot(-c\nabla\phi - \nabla c) + \alpha_+ \mathbf{u}\cdot\nabla c + \alpha_+\frac{\partial c}{\partial t} = 0, \tag{A1}$$

$$\nabla\cdot(c\nabla\phi - \nabla c) + \alpha_- \mathbf{u}\cdot\nabla c + \alpha_-\frac{\partial c}{\partial t} = 0, \tag{A2}$$

where electro-neutrality has been taken into account so that the concentrations of positive and negative ions are equal $c_+ = c_- = c$. The nondimensional parameters α_+ and α_- are the reciprocals of the nondimensional diffusion constants D_+ and D_- of positive and negative ions, respectively. Adding and substracting equations (A1) and (A2), we get

$$D\nabla^2 c = \mathbf{u}\cdot\nabla c + \frac{\partial c}{\partial t}, \tag{A3}$$

$$\nabla\cdot(c\nabla\phi) = \gamma\left(\frac{\partial c}{\partial t} + \mathbf{u}\cdot\nabla c\right), \tag{A4}$$

where $D = 2/(\alpha_+ + \alpha_-)$ and $\gamma = (\alpha_+ - \alpha_-)/2$. Equation (A3) is the diffusion equation for the salt concentration, with D a nondimensional ambipolar diffusion constant. Equation (A4) can be read as the equation for the electrical potential where γ is a parameter that controls the ion mobility asymmetry.

The boundary conditions on the surface of the charged dielectric object are the following [14]. Zero normal flux of co-ions (anions in our case)

$$c\frac{\partial\phi}{\partial n} - \frac{\partial c}{\partial n} = 0. \tag{A5}$$

The normal flux of counter-ions (cations in our case) equate the surface divergence of EDL cation fluxes

$$-c\frac{\partial\phi}{\partial n} - \frac{\partial c}{\partial n} = 2\mathrm{Du}\nabla_s^2(\phi + \ln c), \tag{A6}$$

where Du is the Dukhin number defined as $\mathrm{Du} = (1 + 2\alpha_+)|q_s|\lambda_D$, with q_s and λ_D the nondimensional intrinsic surface charge and Debye length, respectively. Here the normal derivative is from the dielectric to the electrolyte. The Dukhin number is defined in the literature [4] as $\mathrm{Du} = K_s/(\sigma a)$, where K_s is the surface conductance. This expression is fully equivalent to the definition $\mathrm{Du} = (1 + 2\alpha_+)|q_s|\lambda_D$ for symmetrical electrolyte with equal diffusivities and large zeta potential (the case we deal with in this work). The supplementary material contains a detailed derivation of the equivalence of the two definitions [23]. In previous equations, we assumed that the particle is nonpolarizable, i.e. the charge induced in the EDL by the external electric field is negligible. This condition will be examined later.

Liquid velocity and pressure satisfy the Navier-Stokes equation for negligible Reynolds number:

$$\mathrm{Re}\frac{\partial \mathbf{u}}{\partial t} = -\nabla p + \nabla^2 \mathbf{u} + \nabla^2\phi\nabla\phi, \qquad \nabla\cdot\mathbf{u} = 0, \quad \text{(A7)}$$

where the Coulomb term is present because gradients of concentration can lead to induced charge in the bulk, through equation (A4), and the time derivative of velocity is present because it may not be negligible for high frequency.

The boundary conditions on the charged dielectric surface are (i) the wall is impermeable, $\mathbf{u}\cdot\mathbf{n} = 0$, and (ii) there is a slip velocity generated at the EDL [31]

$$\mathbf{u}_s = \zeta\nabla_s\phi - 4\ln\left(\cosh(\zeta/4)\right)\nabla_s c, \quad \text{(A8)}$$

where the zeta potential ζ is related to the intrinsic charge by [1]

$$q_s = 2\sqrt{c}\sinh(\zeta/2). \quad \text{(A9)}$$

Here we see that perturbations of salt concentration lead to perturbations of zeta potential, i.e. $\delta\zeta = -\delta c\tanh(\zeta_0/2)/c_0$.

Following Schnitzer and Yariv [15], we now perform a linear expansion in the parameter Du (which is small in our case): $\phi = \phi_0 + \delta\phi$, $c = c_0 + \delta c$, $\zeta = \zeta_0 + \delta\zeta$, $\mathbf{u} = \mathbf{u}_0 + \delta\mathbf{u}$, with $\delta\phi, \delta c, \delta\zeta, \delta\mathbf{u}$ of the order of Du. In addition, the equations will be simplified in order to obtain an analytical solution.

Consider an applied AC electric field of nondimensional angular frequency ω. The solution at order zero ($\mathrm{Du} = 0$) is: a) the salt concentration is unperturbed, $c_0 = 1$; b) the zeta potential in the absence of concentration polarization is uniform and given by the relation $q_s = 2\sinh(\zeta_0/2)$; c) the potential in the liquid bulk is $\phi_0(t) = \mathcal{R}e[\tilde{\phi}_0 e^{i\omega t}]$, where $\tilde{\phi}_0$ is the potential phasor that satisfies Laplace's equation with boundary condition $\partial\tilde{\phi}_0/\partial n = 0$ at the dielectric surface (the solution for a cylinder is given in equation (2)); and d) the velocity field and pressure are, respectively, $\mathbf{u}_0(t) = \mathcal{R}e[\tilde{\mathbf{u}}_0 e^{i\omega t}]$ and $p_0(t) = \mathcal{R}e[\tilde{p}_0 e^{i\omega t}]$, where $\tilde{\mathbf{u}}_0$ and $\tilde{p}_0$ satisfy

$$i\omega\mathrm{Re}\tilde{\mathbf{u}}_0 = -\nabla\tilde{p}_0 + \nabla^2\tilde{\mathbf{u}}_0, \qquad \nabla\cdot\tilde{\mathbf{u}}_0 = 0, \quad \text{(A10)}$$

with boundary condition $\tilde{\mathbf{u}}_0 = \zeta_0\nabla\tilde{\phi}_0$ at the dielectric surface. The analytical solution for the velocity and pressure generated around a cylinder is shown below (Appendix D).

The concentration δc satisfies

$$D\nabla^2\delta c = \mathbf{u}_0\cdot\nabla\delta c + \frac{\partial\delta c}{\partial t}. \quad \text{(A11)}$$

Here we neglect the advection term in order to obtain an analytical solution. For this to be valid, the Peclet (Pe) number must be negligibly small ($Pe = U_0 L/\bar{D}$, where U_0 is a typical velocity, L is the characteristic length for the concentration gradients and $\bar{D}$ the dimensional diffusivity of the ions). For DC, the characteristic length is a, the pillar radius. For AC fields, the characteristic length is the smaller of a or the diffusion penetration depth (the penetration depth is $\sqrt{\bar{D}/\bar{\omega}}$, with $\bar{D}$ and $\bar{\omega}$ dimensional quantities). Pe is negligible when either U_0 or L is very small. In our experimental system, this implies that either U_0 is much smaller than $200\,\mu m/s$ or $\omega \gg 2\pi 10\,\mathrm{rad/s}$. The boundary condition for equation (A11) at the dielectric surface is

$$-\frac{\partial\delta c}{\partial n} = \mathrm{Du}\nabla_s^2(\phi_0). \quad \text{(A12)}$$

Since ϕ_0 is an oscillating function in time with angular frequency ω and we neglect the advection term, we find a solution of δc that is of the form $\delta c = \mathcal{R}e[\delta\tilde{c}e^{i\omega t}]$. The complex function $\delta\tilde{c}$ satisfies

$$D\nabla^2\delta\tilde{c} = i\omega\delta\tilde{c}. \quad \text{(A13)}$$

with boundary condition

$$\frac{\partial\delta\tilde{c}}{\partial n} = -\mathrm{Du}\nabla_s^2(\tilde{\phi}_0). \quad \text{(A14)}$$

We further assume that positive and negative ions have the same mobility so that $\gamma = 0$ in equation (A4). The potential $\delta\phi$ satisfies then

$$\nabla^2\delta\phi + \nabla\phi_0\cdot\nabla\delta c = 0, \quad \text{(A15)}$$

with boundary condition on the dielectric surface

$$\frac{\partial\delta\phi}{\partial n} = \frac{\partial\delta c}{\partial n}. \quad \text{(A16)}$$

Equation (A15) and b.c. (A16) implies that the general solution for $\delta\phi$ has three Fourier independent frequency components: $\left\{1, e^{i\omega t}, e^{2i\omega t}\right\}$. We are interested in the time-independent component, because this contributes to the rectified velocity, as shown below. Thus we solve

$\nabla^2\langle\delta\phi\rangle + \langle\nabla\phi_0\cdot\nabla\delta c\rangle = 0.$

The time-averaged velocity and pressure at the first order satisfy

$$\nabla^2\delta\mathbf{u} + \langle\nabla^2\delta\phi\nabla\phi_0\rangle = \nabla\delta p, \qquad \nabla\cdot\delta\mathbf{u} = 0. \tag{A17}$$

The Coulomb term has zero time average, $\langle\nabla^2\delta\phi\nabla\phi_0\rangle = 0$. Effectively, the Laplacian of $\delta\phi$ is equal to $-\nabla\phi_0\cdot\nabla\delta c$ because of equation (A15). It has Fourier components $\left\{1, e^{2i\omega t}\right\}$ and when multiplied by $\nabla\phi_0$ the Coulomb term has Fourier components $\left\{e^{i\omega t}, e^{3i\omega t}\right\}$.

The boundary conditions for the time-averaged velocity on the dielectric surface at the first order are $\delta\mathbf{u}\cdot\mathbf{n} = 0$ and the time-averaged slip velocity

$$\delta\mathbf{u}_s = \zeta_0\nabla_s\langle\delta\phi\rangle + \langle\delta\zeta\nabla_s\phi_0\rangle - 4\ln\left(\cosh(\zeta_0/4)\right)\nabla_s\langle\delta c\rangle = \\ \cdots = \zeta_0\nabla_s\langle\delta\phi\rangle + \langle\delta\zeta\nabla_s\phi_0\rangle, \tag{A18}$$

where the last equality comes from $\langle\delta c\rangle = 0$. Here $\delta\zeta = -\delta c\tanh(\zeta_0/2)$.

Summary of approximations in the model:

1. Thin EDL and highly charged surface, as required for the Schnitzer-Yariv model;
2. Frequencies much smaller than the electrolyte charge relaxation frequency, ensuring that the EDL is in quasi-equilibrium;
3. High frequencies or weak electric fields so that advection of ions can be neglected;
4. Small Du to justify the use of a linear expansion;
5. Equal ion diffusivities so that the charge induced in the bulk due to different diffusivities can be neglected;
6. Negligible induced charge in the EDL (valid for common dielectrics).

Appendix B: Negligible induced charge

At this point we examine the charge induced by the applied field on a dielectric cylinder. First we compare the maximum induced zeta potential from the induced charge on a dielectric and also from the change in concentration due to surface conduction. Both induced zeta potentials are maximum at zero frequency. According to [20] the maximum induced zeta potential on a dielectric cylinder due to induced charge is

$$\zeta_{IC} = 2\frac{\varepsilon_d}{\varepsilon_w}E_0\lambda_D, \tag{B1}$$

where ε_d and ε_w are the dielectric constants of the solid and water, respectively. From $\delta\zeta = -\delta c\tanh(\zeta_0/2)$ with δc given by eq. (5) in nondimensional form and evaluated on the cylinder surface, the maximum induced zeta potential due to the concentration perturbation is

$$\zeta_{CP} = 2\mathrm{Du}E_0\tanh(|\zeta_0|/2), \tag{B2}$$

We see that for thin EDL ($\lambda_D \ll 1$) and a non-negligible Dukhin number (i.e. Du$>\lambda_D$), $\zeta_{IC}/\zeta_{CP} \sim (\varepsilon_d/\varepsilon_w)(\lambda_D/\mathrm{Du}) \ll 1$ for common dielectrics. Thus, it is justifiable to neglect ζ_{IC} compared with ζ_{CP}.

Appendix C: Functions for analytical solution

The functions $F(r)$ and $G(r)$ are obtained from the equations:

$$\frac{1}{r}\frac{\partial}{\partial r}\left(r\frac{\partial F}{\partial r}\right) = f, \tag{C1}$$

$$\frac{1}{r}\frac{\partial}{\partial r}\left(r\frac{\partial G}{\partial r}\right) - \frac{4G}{r^2} = g, \tag{C2}$$

with boundary conditions of $\partial F/\partial r = \partial G/\partial r = 0$, both for $r = 1$ and $r\to\infty$. Only the function $G(r)$ contributes to the rectified slip velocity (equation 12). We solve for G using Green's function that satisfies equation (C2) but with source equal to the Dirac delta function $\delta(r-r')$ and with boundary conditions of zero radial derivatives at $r = 1$ and $r\to\infty$. The solution for G is then

$$G(r) = -r^{-2}\int_1^r \frac{g(r')(r'^4+1)}{4r'}dr' - (r^2+r^{-2})\int_r^\infty \frac{g(r')}{4r'}dr'. \tag{C3}$$

According to equation (12), we require the value of G evaluated on the cylinder surface $G(1)$:

$$G(1) = -\int_1^\infty \frac{g(r')}{2r'}dr' = \frac{1}{4K_1'(k)}\int_1^\infty\left(\frac{K_0(kr')}{r'^3} - \frac{K_2(kr')}{r'}\right)dr'. \tag{C4}$$

The integral (C4) is evaluated using Mathematica.

Appendix D: Oscillating velocity and pressure around a cylinder

This appendix derives the oscillating velocity at zero order. This does not affect the stationary electroosmotic velocity since we have neglected the advection term in equation (5). The solution to equation (A10) for the case of a cylinder can be found by writing [32]

$$\tilde{\mathbf{u}}_0 = -\frac{\nabla\tilde{p}_0}{i\omega\mathrm{Re}} + \nabla\times(\psi\hat{z}), \tag{D1}$$

with equations for $\tilde{p}_0$ and ψ given by, respectively,

$$\nabla^2\tilde{p}_0 = 0, \qquad \nabla^2\psi = i\omega\mathrm{Re}\psi \tag{D2}$$

Imposing boundary conditions of zero velocity at infinity and slip velocity on the cylinder surface $\tilde{\mathbf{u}}_0 = 2\zeta E_0 \sin\theta\hat{\theta}$ leads to

$$\tilde{p}_0 = i\omega \mathrm{Re} 2\zeta E_0 \frac{K_1(\alpha)}{K_1(\alpha)+\alpha K_1'(\alpha)}\frac{\cos\theta}{r}, \tag{D3}$$

$$\psi = -2\zeta E_0 \frac{K_1(\alpha r)}{K_1(\alpha)+\alpha K_1'(\alpha)}\sin\theta, \tag{D4}$$

where $\alpha = \sqrt{i\omega \mathrm{Re}}$.

[1] R.J. Hunter, *Introduction to Modern Colloid Science* (Oxford University Press, 1993).

[2] J. Lyklema, *Fundamentals of Interface and Colloid Science* (Academic Press Limited, 1995).

[3] H.A. Stone, A.D. Stroock, and A. Ajdari, "Engineering flows in small devices: Microfluidics toward a lab-on-a-chip," Annu. Rev. Fluid Mech. **36**, 381411 (2004).

[4] Angel V. Delgado, Fernando Gonzalez-Caballero, R.J. Hunter, L.K. Koopal, and J. Lyklema, "Measurement and interpretation of electrokinetic phenomena (IUPAC technical report)," Pure and Applied Chemistry **77**, 1753–1802 (2005).

[5] Victor Calero, Pablo Garcia-Sanchez, Antonio Ramos, and Hywel Morgan, "Electrokinetic biased deterministic lateral displacement: Scaling analysis and simulations," Journal of Chromatography A , 461151 (2020).

[6] Yuval Eckstein, Gilad Yossifon, Avraham Seifert, and Touvia Miloh, "Nonlinear electrokinetic phenomena around nearly insulated sharp tips in microflows," Journal of colloid and interface science **338**, 243–249 (2009).

[7] Sunil Kumar Thamida and Hsueh-Chia Chang, "Nonlinear electrokinetic ejection and entrainment due to polarization at nearly insulated wedges," Physics of Fluids **14**, 4315–4328 (2002).

[8] Paul Takhistov, Ksenia Duginova, and Hsueh-Chia Chang, "Electrokinetic mixing vortices due to electrolyte depletion at microchannel junctions," Journal of colloid and interface science **263**, 133–143 (2003).

[9] Matan Zehavi, Alicia Boymelgreen, and Gilad Yossifon, "Competition between induced-charge electro-osmosis and electrothermal effects at low frequencies around a weakly polarizable microchannel corner," Physical Review Applied **5**, 044013 (2016).

[10] M. Z. Bazant and T. M. Squires, "Induced-charge electrokinetic phenomena: theory and microfluidic applications," Physical Review Letters **92**, 066101 (2004).

[11] S.S Dukhin and Vladimir Nikolaievich Shilov, *Dielectric phenomena and the double layer in disperse systems and polyelectrolytes* (John Wiley and Sons, 1974).

[12] VN Shilov, AV Delgado, F Gonzalez-Caballero, and C Grosse, "Thin double layer theory of the wide-frequency range dielectric dispersion of suspensions of non-conducting spherical particles including surface conductivity of the stagnant layer," Colloids and Surfaces A: Physicochemical and Engineering Aspects **192**, 253–265 (2001).

[13] Nataliya A Mishchuk, "Concentration polarization of interface and non-linear electrokinetic phenomena," Advances in Colloid and Interface Science **160**, 16–39 (2010).

[14] Ory Schnitzer and Ehud Yariv, "Macroscale description of electrokinetic flows at large zeta potentials: nonlinear surface conduction," Physical Review E **86**, 021503 (2012).

[15] Ory Schnitzer and Ehud Yariv, "Nonlinear electrophoresis at arbitrary field strengths: small-Dukhin-number analysis," Physics of Fluids **26**, 122002 (2014).

[16] Constantino Grosse and Vladimir Nikolaievich Shilov, "Theory of the low-frequency electrorotation of polystyrene particles in electrolyte solution," Journal of Physical Chemistry **100**, 1771–1778 (1996).

[17] Constantino Grosse and Vladimir Nikolaievich Shilov, "Theory of the low frequency electrorotation of disperse particles in electrolyte solution," Colloids and Surfaces A: Physicochemical and Engineering Aspects **140**, 199–207 (1998).

[18] Veniamin G. Levich, *Physicochemical Hydrodynamics* (Prentice-Hall, 1962).

[19] John S. Newman and Karen E. Thomas-Alyea, *Electrochemical systems* (Wiley-IEEE, 2004).

[20] Todd M Squires and Martin Z Bazant, "Induced-charge electro-osmosis," Journal of Fluid Mechanics **509**, 217–252 (2004).

[21] G Yossifon, I Frankel, and T Miloh, "Macro-scale description of transient electro-kinetic phenomena over polarizable dielectric solids," Journal of fluid mechanics **620**, 241 (2009).

[22] Cunlu Zhao and Chun Yang, "Analysis of induced-charge electro-osmotic flow in a microchannel embedded with polarizable dielectric blocks," Physical Review E **80**, 046312 (2009).

[23] See Supplemental Material at [URL will be inserted by publisher].

[24] Alice Sze, David Erickson, Liqing Ren, and Dongqing Li, "Zeta-potential measurement using the smoluchowski equation and the slope of the current–time relationship in electroosmotic flow," Journal of colloid and interface science **261**, 402–410 (2003).

[25] Mario A Saucedo-Espinosa and Blanca H Lapizco-Encinas, "Refinement of current monitoring methodology for electroosmotic flow assessment under low ionic strength conditions," Biomicrofluidics **10**, 033104 (2016).

[26] Irina Ermolina and Hywel Morgan, "The electrokinetic properties of latex particles: comparison of electrophoresis and dielectrophoresis," Journal of colloid and interface science **285**, 419–428 (2005).

[27] Martina Viefhues, S Manchanda, T-C Chao, Dario Anselmetti, Jan Regtmeier, and Alexandra Ros, "Physisorbed

surface coatings for poly (dimethylsiloxane) and quartz microfluidic devices," Analytical and bioanalytical chemistry **401**, 2113 (2011).

[28] Qianru Wang, Naga Neehar Dingari, and Cullen R Buie, "Nonlinear electrokinetic effects in insulator-based dielectrophoretic systems," Electrophoresis **38**, 2576–2586 (2017).

[29] Blanca H Lapizco-Encinas, Blake A Simmons, Eric B Cummings, and Yolanda Fintschenko, "Insulator-based dielectrophoresis for the selective concentration and separation of live bacteria in water," Electrophoresis **25**, 1695–1704 (2004).

[30] Victor Calero, Pablo Garcia-Sanchez, Carlos Honrado, Antonio Ramos, and Hywel Morgan, "Ac electrokinetic biased deterministic lateral displacement for tunable particle separation," Lab on a Chip **19**, 1386–1396 (2019).

[31] DC Prieve, JL Anderson, JP Ebel, and ME Lowell, "Motion of a particle generated by chemical gradients. part 2. electrolytes," Journal of Fluid Mechanics **148**, 247–269 (1984).

[32] J Milton Andres and Uno Ingard, "Acoustic streaming at low reynolds numbers," The Journal of the Acoustical Society of America **25**, 932–938 (1953).

[33] R. Lindken, M. Rossi, S. Große, and J. Westerweel, "Micro-particle image velocimetry (PIV): Recent developments, applications and guidelines," Lab on a Chip **9**, 2551–2567 (2009).

[34] M. Raffel, C. E. Willert, F. Scarano, C. J. Kähler, S. T. Wereley, and J. Kompenhans, *Particle Image Velocimetry: A Practical Guide*, 3rd ed. (Springer International Publishing AG, 2018).

[35] C. E. Willert and M. Gharib, "Digital particle image velocimetry," Experiments in Fluids **10**, 181–193 (1991).

[36] W. Thielicke, "PIVlab - particle image velocimetry (PIV) tool, matlab central file exchange." .

[37] W. Thielicke and E. J. Stamhuis, "PIVlab towards user-friendly, affordable and accurate digital particle image velocimetry in MATLAB," Journal of Open Research Software **2** (2014), 10.5334/jors.bl.

[38] C. D. Meinhart, S. T. Wereley, and J. G. Santiago, "A PIV algorithm for estimating time-averaged velocity fields," Journal of Fluids Engineering **122**, 285–289 (2000).

[39] M. G. Olsen and R. J. Adrian, "Out-of-focus effects on particle image visibility and correlation in microscopic particle image velocimetry," Experiments in Fluids **29**, S166–S174 (2000).